Measuring primordial non-Gaussianity through weak lensing peak counts

Laura Marian[1], Stefan Hilbert[1], Robert E. Smith[2,1], Peter Schneider[1], Vincent Desjacques[2]

Argelander-Institut für Astronomie, Universität Bonn, Bonn, D-53121, Germany [1]
Institute for Theoretical Physics, University of Zürich, Zürich, CH 8037, Switzerland[2]

We explore the possibility of detecting primordial non-Gaussianity of the local type using weak lensing peak counts. We measure the peak abundance in sets of simulated weak lensing maps corresponding to three models $f_{\rm NL} = 0, -100, 100$. Using survey specifications similar to those of EUCLID and without assuming any knowledge of the lens and source redshifts, we find the peak functions of the non-Gaussian models with $f_{\rm NL} = \pm 100$ to differ by up to 15% from the Gaussian peak function at the high-mass end. For the assumed survey parameters, the probability of fitting an $f_{\rm NL} = 0$ peak function to the $f_{\rm NL} = \pm 100$ peak functions is less than 0.1%. Assuming the other cosmological parameters known, $f_{\rm NL}$ can be measured with an error $\Delta f_{\rm NL} \approx 13$. It is therefore possible that future weak lensing surveys like EUCLID may detect primordial non-Gaussianity from the abundance of peak counts.

Introduction— The inflationary paradigm is the leading theory of the early Universe, of fundamental interest for cosmology and particle physics. Understanding the mechanism and energy scale of inflation remain major goals to attain, despite the continuous and fervent efforts invested in this field.

A measurement of primordial gravitational waves would pin down the energy scale of inflation, though it still belongs to the not-so-near future. One possible way to discriminate between single- and multi-field inflation models is to test the Gaussianity of the primordial density fluctuations [1]. The Cosmic Microwave Background (CMB) has been so far the main and cleanest inflationary probe. Recent results from the Wilkinson Microwave Anisotropy Probe (WMAP) [2] established the existence at the 1σ-level of primordial non-Gaussianity of the local type, defined by the equation:

$$\Phi(\boldsymbol{x}) = \phi(\boldsymbol{x}) + f_{\rm NL}[\phi^2(\boldsymbol{x}) - \langle\phi^2(\boldsymbol{x})\rangle]. \qquad (1)$$

The parameter $f_{\rm NL}$ quantifies the local quadratic deviation of the Bardeen potential Φ from a Gaussian potential ϕ, and it is currently constrained to the value 32 ± 21 [2].

It has long been suggested [3–6] that low-redshift observables can also be used to measure primordial non-Gaussianity, despite the fact that the density field at such redshifts is strongly non-Gaussian due to the action of gravity. In the local non-Gaussianity models, there are mainly two effects on low-redshift observables as recently outlined in the comprehensive study of [7], and further explored in [8–12]. First, $f_{\rm NL}$ induces a scale-dependence in the bias of dark matter halos, which affects primarily the largest scales, i.e. $k < 0.02\,h\,{\rm Mpc}^{-1}$. Thus one can in principle separate the $f_{\rm NL}$ scale dependence from the gravitational one, which occurs on smaller scales. Second, the abundance of massive halos is higher/lower for positive/negative values of $f_{\rm NL}$ [6, 13].

In this paper we shall numerically investigate the sensitivity of weak gravitational lensing (WL) peak counts to primordial non-Gaussianity of the local type. The potential of WL surveys to constrain $f_{\rm NL}$ has already been tackled [14–16], though without considering shear peaks. Peak counts are a natural candidate for $f_{\rm NL}$ studies, since the largest of them are caused primarily by massive halos. Should peak counts prove to be a sensitive $f_{\rm NL}$ probe, then one could easily use large future surveys like EUCLID [17] or the Large Synoptic Survey Telescope (LSST) [18] to obtain low-redshift constraints on primordial non-Gaussianity.

Method—We study simulated WL convergence maps created from ray-tracing through a suite of N-body simulations, generated with the publicly available code GADGET [19]. A subset of these simulations was used and described in the work of [8]. Three values of $f_{\rm NL}$ are considered: 0, -100, +100, while the other cosmological parameters are kept fixed. The cosmology matches the WMAP5 results [20]. We have a total of 18 simulations, with 6 realizations per $f_{\rm NL}$ value. The initial conditions for each of the 6 sets of $f_{\rm NL}$-model realizations are matched to reduce the cosmic variance on the comparison of the peak functions corresponding to each model. The box size is 1600 h^{-1} Mpc, the number of particles is $N = 1024^3$, and the softening length is $l_{\rm soft} = 40\,h^{-1}$ kpc.

We consider a EUCLID-like survey [17] for the WL simulations with: an rms $\sigma_\gamma = 0.3$ for the intrinsic image ellipticity, a source number density $\bar{n}_{\rm gal} = 40\,{\rm arcmin}^{-2}$, and a redshift distribution of source galaxies given by $\mathcal{P}(z) = 1.5\,z^2/z_0^3\,\exp[-(z/z_0)^{1.5}]$, where $z_0 = 0.6$. The mean redshift of this distribution is $z_{\rm mean} = 0.9$.

From each N-body simulation we generate 16 independent fields of view. Each field has an area of $12 \times 12\,{\rm deg}^2$ and is tiled by 4096^2 pixels, yielding an angular resolution $\theta_{\rm pix} = 10\,{\rm arcsec}$ and a total area of $\approx 14000\,{\rm deg}^2$ for each $f_{\rm NL}$ model. The effective convergence κ in each pixel is calculated by tracing a light ray back through the simulation with a Multiple-Lens-Plane ray-tracing algorithm [21, 22]. Gaussian shape noise with variance $\sigma_\gamma^2/(\bar{n}_{\rm gal}\,\theta_{\rm pix}^2)$ is then added to each pixel [23].

For the peak finding we use an aperture filter [24], matching an Navarro-Frenk-White (NFW) profile [25]

convolved with a Gaussian function. The width of the latter is $f \times l_{\rm soft}$, where $f = 1.5$ for $M < 7 \times 10^{14}\, h^{-1}\, {\rm M}_\odot$ and $f = 2$ otherwise. Thus we adopt the convergence model: $\kappa_{\rm model} = \kappa_{\rm NFW} \circ f_{\rm Gauss}$, which agrees very well with the measured convergence profiles of the peaks in the maps. The model is useful both when working with simulations, since it accounts for the lack of resolution below the softening scale, and also when using real data, since shear data is difficult to obtain near the centres of clusters.

The amplitude of the smoothed field at a point $\boldsymbol{x_0}$ is given by:

$$\hat{M}(\boldsymbol{x_0}) = \int d^2x\, W(\boldsymbol{x_0} - \boldsymbol{x})\kappa(\boldsymbol{x}), \qquad (2)$$

where W is our filter and κ is the convergence field. The filter W can be written as follows:

$$W(x) = \mathcal{C}_{\rm W}\, \frac{\kappa_{\rm model}(x) - \bar{\kappa}_{\rm model}(R)}{\sigma_\gamma^2/\bar{n}_{\rm gal}}, \qquad (3)$$

where $\mathcal{C}_{\rm W}$ is a normalization constant and R is the aperture radius, i.e. the radius over which the filter is compensated. We choose the normalization constant to be:

$$\mathcal{C}_{\rm W} = \frac{\sigma_\gamma^2}{\bar{n}_{\rm gal}}\, \frac{M_{\rm NFW}}{\int d^2x\, \kappa^2_{\rm model}(x) - \pi R^2\, \bar{\kappa}^2_{\rm model}(R)}\,. \qquad (4)$$

If $\boldsymbol{x_0}$ is the location of a peak created by an NFW cluster of mass $M_{\rm NFW}$ and redshift z, and the convergence field is smoothed with a filter tuned to precisely such a cluster, i.e. $\kappa_{\rm model}$ in Eq. (3) corresponds to the same $M_{\rm NFW}$ and z, then this filter returns a maximum S/N at $\boldsymbol{x_0}$. At this location, the amplitude of the smoothed map is:

$$\hat{M}(\boldsymbol{x_0}|M_{\rm NFW}, z) = M_{\rm NFW}\,. \qquad (5)$$

The peak is assigned the mass $M_{\rm NFW}$. In practice, we smooth the convergence field with filters of various masses, which yield different amplitudes (larger and smaller than the filter mass) at the location of peaks. We interpolate these amplitudes to determine the filter mass that would satisfy Eq. (5).

We choose R to be the virial radius of the cluster to which the filter is tuned: $R = (3M_{\rm NFW}/800\,\pi\,\bar{\rho})^{1/3}$, where $\bar{\rho}$ is the mean density of the universe. Thus a filter at a given redshift can be specified either through the mass $M_{\rm NFW}$ or through its size R. We adopt the mass convention of Sheth-Tormen [26], with an overdensity defined as 200 $\times$ the mean density (not the critical density). The NFW profile that defines $\kappa_{\rm model}$ is also truncated at R, as described for instance by [27]. We evaluate the S/N of the mass estimator in a simplified scenario where we ignore projection effects, and consider only the intrinsic ellipticity noise. In this case the variance of the estimator is given by: ${\rm Var}(\hat{M}) = M_{\rm NFW}\,\mathcal{C}_{\rm W}$, and the S/N is obtained by combining this with the above equations.

Finally, in the case where no shape noise is included, we use the same filter as in our previous work [28]. This filter can also be obtained by formally taking $\sigma_\gamma^2/\bar{n}_{\rm gal} = 1$ in Eqs (3), (4) above, and it is no longer an optimal filter. The analysis of the convergence maps is carried out in two situations: with and without shape noise. We adopt a very conservative approach in which we consider known only the redshift distribution of the source galaxies and the shape noise level, without any other information on the sources or on the detected peaks. We also do not resort to tomographic techniques. While this is an overly-pessimistic scenario for a next-generation lensing survey like EUCLID, our goal here is to provide a proof of concept of the possibility of using WL peak counts to constrain primordial non-Gaussianity, rather than the final quantitative answer to this question.

We perform a hierarchical smoothing of the maps with filters of various sizes, from the largest down to the smallest, as described in [28, 29]. This approach removes the problem of 'peaks-in-peaks' and it also naturally eliminates the dependence of the measured peak function on a particular filter scale. Since the mean redshift of the source distribution is 0.9, we adopt a fixed redshift of 0.3 for the matched filter described above. For this redshift, the scale of the filter varies from corresponding masses of $2 \times 10^{15}\, h^{-1}\, {\rm M}_\odot$ to $3 \times 10^{13}\, h^{-1}\, {\rm M}_\odot$ in the absence of shape noise, and $10^{14}\, h^{-1}\, {\rm M}_\odot$ in the presence of it. The latter lower-limit choice of the filter scale is due to the fact that shape noise contaminates seriously the smaller peaks; imposing a minimum S/N threshold alleviates but does not remove the contamination. Peaks are detected in the smoothed maps as local maxima, and are assigned a mass as described in the previous section.

Results—Figure 1 presents the main result of this work. The upper panels illustrate the peak functions measured in the $f_{\rm NL} = \pm 100$ cosmologies, in the absence (left panel) and presence of shape noise (right panel). For each $f_{\rm NL}$ model, the points are the average of the peak counts measured in all 96 fields and the error bars represent errors on the mean. In the case of shape noise, we select only peaks with a $S/N > 3$. We note that the two average peak functions are clearly distinct at the high-mass end, i.e. for $M > 3 \times 10^{14}\, h^{-1}\, {\rm M}_\odot$. This is better seen in the lower panels which show the difference of the peak abundance measured in the $f_{\rm NL} = \pm 100$ cosmologies, relative to the $f_{\rm NL} = 0$ peak abundance. The error bars do not reflect the matched initial conditions of the Gaussian and the $f_{\rm NL}$ models: the fractional difference is computed as an average of the $f_{\rm NL} \pm 100$ peak abundance in each field ratioed to *the average* Gaussian peak abundance (which represents our best model for the true Gaussian peak abundance), as opposed to the average of the ratio of the non-Gaussian and Gaussian peak functions measured in the same field. The latter would have removed the cosmic variance of the fractional difference.

Just like in the case of the 3D halo mass function,

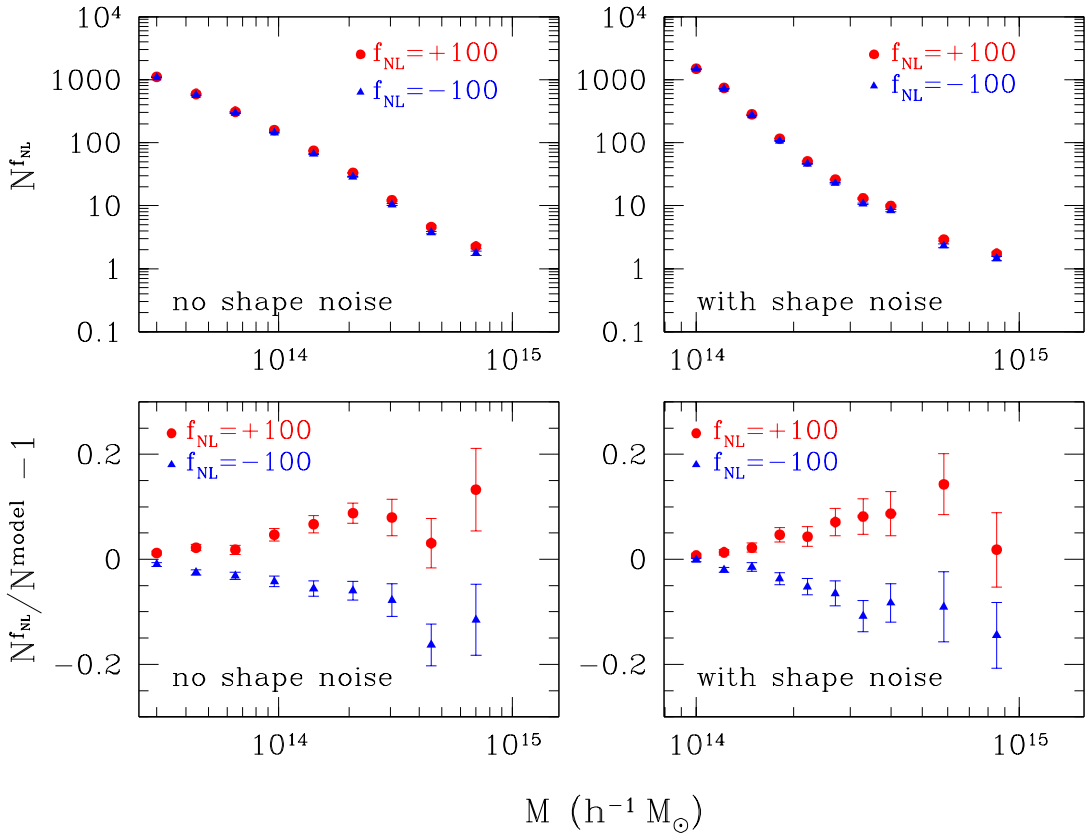

FIG. 1: *Upper panels*: The measured peak functions for $f_{\rm NL}=+100$ (red circles) and $f_{\rm NL}=-100$ (blue triangles) for a survey with a mean redshift $z_{\rm mean}=0.9$ and an area of 14000 deg^2. The filter used corresponds to redshift 0.3. The peak functions in the left panel are measured in the absence of shape noise, while in the right panel shape noise is included (assuming 40 galaxies/arcmin^2), and only the peaks with a $S/N>3$ were selected (hence the smaller mass range on the x-axis).

Lower panels: The fractional difference of the peak functions for the $f_{\rm NL}=\pm100$ models and the Gaussian model (red circles/blue triangles), without/with shape noise (left/right panel). The points are obtained as an average over all the fields of the fractional difference of the $f_{\rm NL}\pm100$ peak functions in every field and *the average* peak function in the Gaussian model.

(see for example [8, 12]), the peak functions for the $f_{\rm NL}$ models show a deviation from the Gaussian case. Unlike the 3D studies which have presented halo mass functions measured at a single redshift, the peak functions that we show here combine peaks in the redshift range of the source distribution, and therefore are not as regular and symmetric as their 3D counterparts. The asymmetry is most likely due to modifications of the S/N of peaks by line-of-sight projections, and also by shape noise contamination. The trend is similar however, with high-mass peaks displaying the largest deviation. For both $f_{\rm NL}$ models, this is about 10-15% for the largest mass bins i.e. $M>4\times10^{14}\,h^{-1}\,{\rm M}_\odot$.

To quantify the significance of the deviation, we perform a χ^2-test. For the fiducial model $f_{\rm NL}=0$, we estimate the covariance of the counts in a field. We use the covariance of the mean to obtain the χ^2. For both $f_{\rm NL}\pm100$ we find a probability $<0.1\%$ to fit the $f_{\rm NL}\pm100$ peak functions with an $f_{\rm NL}=0$ peak function. This is also true if we consider only the diagonal elements (the variance of the mass bins) instead of the full covariance matrix, and also if we vary the mass bins. We also use the measured counts to estimate the Fisher error that a 14000 deg^2 WL survey would yield on $f_{\rm NL}$. Assuming all other cosmological parameters known, the forecasted error is $\Delta f_{\rm NL}\approx13$ for the fiducial value $f_{\rm NL}=0$. The values of the χ^2 and the Fisher error are largely maintained also if we completely eliminate the reduction in the cosmic variance due to the matching of the initial conditions, by using the first three simulations to compute the $f_{\rm NL}=+100$ peak function and the last three for the $f_{\rm NL}=-100$ function.

Though these results are already very encouraging, it is possible to improve measurements of primordial non-Gaussianity from WL surveys even if one considers only peak counts. The most important is probably the use of tomography, as numerical and analytical studies of the 3D mass functions have shown that deviations of the halo abundance from the Gaussian case significantly increase with redshift. Tomography would allow peaks to

be separated not only in terms of their S/N–mass, but also of their redshifts, thus acquiring more sensitivity to $f_{\rm NL}$. Our immediate goals are to further study how WL can be used to constrain primordial non-Gaussianity, to build improved $f_{\rm NL}$ estimators from WL observables, and to forecast $f_{\rm NL}$ constraints based on these observables.

For now we convey a simple, yet powerful statement: future WL surveys can detect primordial non-Gaussianity of the local type from at least one statistic–peak counts. In particular, a EUCLID-type survey should convincingly achieve this purpose.

[1] P. Creminelli and M. Zaldarriaga, Journal of Cosmology and Astro-Particle Physics **10**, 6 (2004), arXiv:astro-ph/0407059.

[2] E. Komatsu, K. M. Smith, J. Dunkley, C. L. Bennett, B. Gold, G. Hinshaw, N. Jarosik, D. Larson, M. R. Nolta, L. Page, et al., ArXiv e-prints (2010), 1001.4538.

[3] B. Grinstein and M. B. Wise, Astrophys. J. **310**, 19 (1986).

[4] F. Lucchin and S. Matarrese, Astrophys. J. **330**, 535 (1988).

[5] J. N. Fry and R. J. Scherrer, Astrophys. J. **429**, 36 (1994).

[6] S. Matarrese, L. Verde, and R. Jimenez, Astrophys. J. **541**, 10 (2000), arXiv:astro-ph/0001366.

[7] N. Dalal, O. Doré, D. Huterer, and A. Shirokov, Phys. Rev. D **77**, 123514 (2008), 0710.4560.

[8] V. Desjacques, U. Seljak, and I. T. Iliev, Mon. Not. R. Astron. Soc. **396**, 85 (2009), 0811.2748.

[9] M. Grossi, L. Verde, C. Carbone, K. Dolag, E. Branchini, F. Iannuzzi, S. Matarrese, and L. Moscardini, Mon. Not. R. Astron. Soc. **398**, 321 (2009), 0902.2013.

[10] A. Pillepich, C. Porciani, and O. Hahn, Mon. Not. R. Astron. Soc. **402**, 191 (2010), 0811.4176.

[11] T. Y. Lam and R. K. Sheth, Mon. Not. R. Astron. Soc. **398**, 2143 (2009), 0905.1702.

[12] R. E. Smith, V. Desjacques, and L. Marian, ArXiv e-prints (2010), 1009.5085.

[13] M. Lo Verde, A. Miller, S. Shandera, and L. Verde, Journal of Cosmology and Astro-Particle Physics **4**, 14 (2008), 0711.4126.

[14] A. Amara and A. Refregier, Mon. Not. R. Astron. Soc. **351**, 375 (2004), arXiv:astro-ph/0310345.

[15] F. Pace, L. Moscardini, M. Bartelmann, E. Branchini, K. Dolag, M. Grossi, and S. Matarrese, ArXiv e-prints (2010), 1005.0242.

[16] C. Fedeli and L. Moscardini, Mon. Not. R. Astron. Soc. **405**, 681 (2010), 0912.4112.

[17] A. Refregier, A. Amara, T. D. Kitching, A. Rassat, R. Scaramella, J. Weller, and f. t. Euclid Imaging Consortium, ArXiv e-prints (2010), 1001.0061.

[18] LSST Science Collaborations, P. A. Abell, J. Allison, S. F. Anderson, J. R. Andrew, J. R. P. Angel, L. Armus, D. Arnett, S. J. Asztalos, T. S. Axelrod, et al., ArXiv e-prints (2009), 0912.0201.

[19] V. Springel, Mon. Not. R. Astron. Soc. **364**, 1105 (2005).

[20] E. Komatsu, J. Dunkley, M. R. Nolta, C. L. Bennett, B. Gold, G. Hinshaw, N. Jarosik, D. Larson, M. Limon, L. Page, et al., Astrophys. J. Supp. **180**, 330 (2009), 0803.0547.

[21] S. Hilbert, S. D. M. White, J. Hartlap, and P. Schneider, Mon. Not. R. Astron. Soc. **382**, 121 (2007), arXiv:astro-ph/0703803.

[22] S. Hilbert, J. Hartlap, S. D. M. White, and P. Schneider, Astron. Astrophys. **499**, 31 (2009), 0809.5035.

[23] S. Hilbert, R. B. Metcalf, and S. D. M. White, Mon. Not. R. Astron. Soc. **382**, 1494 (2007), arXiv:0706.0849.

[24] P. Schneider, Mon. Not. R. Astron. Soc. **283**, 837 (1996).

[25] J. F. Navarro, C. S. Frenk, and S. D. M. White, Astrophys. J. **490**, 493 (1997).

[26] R. K. Sheth and G. Tormen, Mon. Not. R. Astron. Soc. **308**, 119 (1999).

[27] T. Hamana, M. Takada, and N. Yoshida, Mon. Not. R. Astron. Soc. **350**, 893 (2004).

[28] L. Marian, R. E. Smith, and G. M. Bernstein, Astrophys. J. **709**, 286 (2010), 0912.0261.

[29] L. Marian, R. E. Smith, and G. M. Bernstein, Astrophys. J. Lett. **698**, L33 (2009), 0811.1991.

Acknowledgements

We kindly thank V. Springel for making public GADGET-2 and for providing his B-FoF halo finder. LM, SH, and PS are supported by the Deutsche Forschungsgemeinschaft (DFG) through the grant MA 4967/1-1, through the Priority Programme 1177 'Galaxy Evolution' (SCHN 342/6 and WH 6/3), and through the Transregio TR33 'The Dark Universe'. RES and VD were partly supported by the Swiss National Foundation under contract 200021-116696/1, the WCU grant R32-2008-000-10130-0, and the UZürich under contract FK UZH 57184001. RES also acknowledges support from a Marie Curie Reintegration Grant and the Alexander von Humboldt Foundation.